International Information and Engineering Technology Association
Advancing the World of Information and Engineering

International Journal of Heat and Technology
Vol. 42, No. 2, April, 2024, pp. 620-636
Journal homepage: http://iieta.org/journals/ijht

Optimizing Gas-Filled Interspaces for a Computational Analysis of the Performance of Double-Glazed Photovoltaic Thermal Hybrid

Djahid Gattal[1*], Rabia Khelif[2]

[1] Laboratory of Research on Industrial Risk Control and Safety, Mechanical Engineering Department, Faculty of Technology, Badji Mokhtar University, Annaba 23005, Algeria
[2] Industrial Mechanics Research, Mechanical Engineering Department, Faculty of Technology, Badji Mokhtar University, Annaba 23005, Algeria

Corresponding Author Email: djahid.gattal@univ-annaba.dz

https://doi.org/10.18280/ijht.420229

Received: 19 February 2024
Revised: 23 March 2024
Accepted: 1 April 2024
Available online: 30 April 2024

Keywords:
Eismann correlation, hybrid photovoltaic thermal (PV-T), natural convective heat loss, study of exergy, the total combined efficiency

ABSTRACT

Reducing losses of energy and destroyed exergy requires optimizing the space between double glazings. Air's poor thermophysical characteristics limit its ability to reduce heat loss in double-glazed Photovoltaic thermal (PV-T) systems. The aim of this study is to investigate how gases like argon, xenon, krypton, sulfur dioxide, and carbon monoxide, when trapped within double glazing and positioned between the inner glass and the absorber (PV model), affect the efficiency, useful heat energy, overall heat loss coefficient, and outlet temperature of the Photovoltaic thermal panel. The research uses the new Eismann correlation to repeatedly measure heat transfer in spaces filled with gases, helping to find the best distances. He also looks into how these gases impact exergy efficiency, destruction energy, and system energy. Among these rare gases, Xenon performs the best in terms of thermal performance, followed by Krypton and Argon when compared to air. Specifically, their total combined efficiency of different filling gases is 49.35% (Xenon), 48.72% (Krypton), 48.02% (Argon), 47.71% (sulfur dioxide), 47.05% (carbon monoxide), and 46.92% (air). The ideal gas-filled spaces for these total combined efficiencies are 5 mm for Xenon, 6 mm for Krypton, 9 mm for Argon and sulfur dioxide, and 10 mm for carbon monoxide and air. The exergy approach confirms these results, showing the same optimal gas-filled space widths.

1. INTRODUCTION

During the 20th century, the demand for energy increased dramatically, primarily met through the utilization of fossil fuels, leading to significant concerns about our environment's sustainability. The excessive burning of fossil fuels not only heightened the release of greenhouse gases but also had a considerable impact on global climate change. Acknowledging the limited availability and adverse effects of fossil fuel sources, modern society is increasingly prioritizing the use of renewable resources to fulfill the escalating energy demands, The emissions analysis shows that the PVT system can save 16.0 tonnes of CO_2 over a 20-year lifetime, which is significantly more than the PV system alone [1]. Solar energy stands out among these alternatives as a sustainable and environmentally friendly option. The growing interest in solar power, particularly in regions abundant in sunlight, has driven the widespread adoption of solar collectors [2-4]. These collectors, commonly employed in residential and agricultural heating systems, are attractive due to their straightforward installation and operational simplicity. However, it's important to note that electrically powered fans are necessary for air circulation within the system. In many developing countries, the agricultural sector consists of numerous isolated farms, small remote villages, and rural areas facing challenges in accessing electricity from the national grid due to technical and economic constraints. Nevertheless, this energy requirement could potentially be met by employing photovoltaic/thermal (PV/T) air collectors [5].

Various studies have investigated the effects of different fin and roughness geometries on enhancing heat transfer in photovoltaic thermal (PVT) collectors. These enhancements aim to increase the surface area and turbulence, while reducing heat leakage through the glazing. Copper is found to be the ideal absorber and fin material due to its high thermal conductivity [6]. The most efficient roughness geometry has been determined to be many V-shaped ribs with gaps [7]. The ideal location of the absorber plate in solar air heater systems can be predicted using computational fluid dynamics (CFD) models, which improve thermal efficiency, Nusselt number, and heat transfer coefficient [8]. Overall, these studies provide valuable insights into optimizing the design and performance of PVT collectors.

Solar photovoltaic-thermal (PV/T) systems using flat plates are a promising technology for decentralized power generation. These systems combine thermal energy production and electricity in a single unit, making them efficient and cost-effective. The literature is replete with studies and comparisons of flat plate PV/T collectors of various designs and configurations [9-12]. A few examples of the variables that affect these systems' efficiency are the collector's area of coverage, the distance between the solar cells and the absorber collector, and the number of passes [13]. Anyway, regarding the use of water, past research on the quantity of glass covers found that while a two-cover sheet-and-tube collector performs marginally better thermally at higher water temperatures than a collector with one cover, the second cover significantly reduces the collector's electrical efficiency [14, 15]. The air that is sandwiched between the two windows also serves as an insulator. Due to the fact that heat and electricity can be produced simultaneously through the integration of photovoltaic (PV) and solar thermal (ST) technologies, photovoltaic thermal (PVT) collectors can help advance sustainable energy. PVT systems, therefore, have two main advantages over separate systems: (i) they increase system efficiency, and (ii) they need less surface area [16].

The actual measurements of free convective heat transfer rates via inclined air layers are discussed in a mathematical formula known as the Hollands et al. [17] equation. Alternatively, the formula can also be utilized to finish the calculation, as ElSherbiny et al. [18], Lately in 2015 Eismann [19] provides a correction parameter and analytically calculated findings for convective heat loss by natural convection.

There have been several research projects and studies on a variety of photovoltaic thermal hybrid (PV-T) designs, such as the investigation by Al-Damook et al. [20] the optimization resulted in improved thermal efficiency from 44.5% to 50.1% and electrical efficiency from 10.0% to 10.5% compared to the baseline design. various studies have recognized the need for unbiased operation of PV/T air heaters and have developed solution methodologies for this purpose [21].

Lamnatou and others review photovoltaic /thermal (PVT) systems with a focus on environmental concerns. PV cells, which transform solar radiation into electricity, and thermal units, which remove heat from the PV panels, are combined to form PVT systems. The systems are installed in tandem and have the option of using air, water, or bi-fluid as their operating fluids. Among other things, they are categorized based on the kind of working fluid circulation. Studies on environmental concerns, such as building-added (BA), building-integrated (BI), and concentrating PVT (CPVT) systems, as well as environmental factors influencing PVT, such as solar concentration, heat transfer fluid type, and PV cell material, are covered in this study. The paper comes to the conclusion that PVT systems can be more affordable if the cost of the thermal unit is minimal and can produce more energy than conventional PV module. Future study in this area is informed by the review, which offers insightful information about the environmental features of PVT systems [22].

In the hot and humid tropical climate of Ghana, Abdul-Ganiyu and colleagues tested a photovoltaic-thermal (PVT) module in comparison to a standard photovoltaic (PV) system. The study aimed to assess the real-life outdoor performance of the PVT module and PV system over the course of a year. The results show that the PVT module had a total output energy of 149.92 kWh/m^2 for electricity and 1087.79 kWh/m^2 for thermal outputs, while the PV module had an annual total output energy of 194.79 kWh/m^2. According to the research, the PVT module shows great promise as an off-grid energy alternative. Additional investigation into solar technology and PVT in particular, is required, according to the report, in Africa to address energy deficits and promote sustainable development. It is necessary to conduct a numerical comparison between the PV and PVT in order to determine the influence of various PVT variables on the comparison, including the inlet temperature, packing factor, and mass flow rate [23].

This research compares various hybrid photovoltaic/thermal (PV/T) collector designs for the environment of Iraq with an emphasis on their electrical and thermal performance, comprising four different air-based hybrid PV/T collector types being manufactured and tested, as well as an examination of their efficiency, temperature readings, air flow rate, and pressure drop. The findings indicate that while model IV has superior electrical efficiency, collector model III has the maximum total efficiency [24]. Miki compared the thermal efficiency and overall energy efficiency of hybrid air-type solar collectors with solar air heaters and found that the 23% light shielding by photovoltaic cells had little effect on the collecting efficiency of the hybrid air-type solar collector [25].

According to the research, the typical PVT collector had a thermal efficiency of 22% and an electrical efficiency of around 15%. At a solar radiation value of 750 W, the electrical efficiency was at its peak, and the PVT collector could produce a maximum power comparable to its performance under regular test conditions [26].

A comparative study was conducted on the performances of four photovoltaic/thermal solar air collectors. The study analyzed different designs and configurations of the collectors, including models I, II, III, and IV. The results showed that the Model III collector had the highest combined efficiency, followed by Models IV and II [5]. Model IV had the best electrical efficiency, while Model III had the lowest pressure drop [24].

The energy and exergy efficiencies of hybrid photovoltaic-thermal (PV/T) air collectors vary depending on the specific design and conditions. Generally, Photovoltaic thermal (PVT) collectors, which combine the functions of a flat plate solar collector and a PV panel, have been the subject of several studies on energy and exergy analysis. The energy and exergy efficiency of air-based PVT collectors ranges from 31% to 94% and 8.7% to 18%, respectively [27]. An electrical efficiency of 10% to 25% and a thermal efficiency of 40% to 75% are typical for PVT collectors. The review's key conclusions are that PVT collectors have an energy efficiency of 40%-70% and an exergy efficiency of 5%-20% [28]. Experimental results from different studies show that overall exergy efficiencies for PVT systems can range from 10.52% to 15.44% [29]. Another study found that the energy efficiency of hybrid PV/T air collectors can vary between 33% and 45%, with exergy efficiency ranging from 11% to 16% [30]. Additionally, a study conducted in a cold climatic condition in India showed that the instantaneous energy efficiency of a hybrid PV/T air collector ranged from 55% to 65%, with exergy efficiency ranging from 12% to 15% [31]. Also Saloux et al. [32] developed an explicit analysis of PV and PV/T systems using the exergy method, with the development of explicit electrical and thermal models to characterize each system. Two thermodynamic diagrams are suggested to illustrate the exergy losses in thermal and electrical energy fluxes, which are determined by combining the energy and exergy balances. Examining a PV/T system in various environmental settings, the methodology determines irreversibility, energy efficiency, and exergy efficiency.

Several articles have examined the predictive power of integrated solar panels and single-channel natural flow heat collectors for a variety of uses. When compared to a standalone photovoltaic pan-el, the efficiency of a PV/T system was discovered to be 6-15% greater, indicating that the two systems work together more effectively [33].

Photovoltaic-thermal panels combine the generation of electricity and hot water, but they suffer from inefficiencies due to convective losses. Several studies have been conducted to optimize convective losses in these panels. Optimizing the distance between panes and using different gases to replace the interior air were the subjects of one study. Xenon gas with optimized spacing showed a significant improvement in the convective heat loss coefficient, but the coefficient of overall heat loss only improved slightly due to radiative losses [34].

There have been a number of investigations into the thermal performance of PV/T hybrid systems with multiple air channels and single-glazing flat plates. The experiments were conducted in different climatic conditions, such as Chennai, India [35]. The studies focused on different modifications to the air channels, including the use of fins, baffles, and ribbed surfaces [36, 37]. Variables including air velocity, the amount of heat transferred from the absorber surface to the air, and the channel's physical geometry were discovered to impact the PV/T hybrid system's performance [38]. The experiments showed that increasing the air mass flow rate enhanced the thermal and photovoltaic efficiencies of the system. The electrical efficiency ranged from 13.70% to 14.27%, while the thermal efficiency ranged from 14.12% to 20.81%. The overall system efficiency was found to be around 64% to 58% for different setups.

Thermal and photovoltaic thermal solar collector performance testing can be carried out in a variety of ways. To account for the wide range of seasonal weather conditions, one method is to conduct outside collection tests over the course of several weeks [39]. Estimates of the collectors' thermal performance parameters are provided by this method. Indoor testing with a solar simulator is another option; it's less labor-intensive, but it could result in inaccurate performance estimates for unglazed PVT collectors [40]. To avoid these mistakes, an approach has been suggested that estimates the real performance of outdoor collectors by combining testing in an indoor solar simulator with a comprehensive numerical model [41]. Thermal performance characteristics can be derived for use in system modeling tools and the collector's design can be optimized with this model [42]. On the other hand, the overall heat loss coefficient plays an important role in the design of solar collectors [43]. By introducing a double glaze system and optimizing the space between the absorber plate and the glass cover, the overall heat loss coefficient can be reduced, resulting in higher collector efficiency [44]. Additionally, the use of gas-filled solar collectors represents a new design approach that can enhance the characteristics of thermal solar collectors [45]. Therefore, by optimizing the gas-filled spaces in double-glazing solar collectors, the useful energy generated by PV/T systems can be improved [46, 47].

The purpose of this research is to analyze the effects of a double-glazed flat-plate photovoltaic-thermal hybrid panel's gas (FPPV-T) used in the glazing interspace performance. From the outset, in order to determine the natural convection transfer coefficients and the extended Eismann correlation [19], the Rayleigh number is utilized as a function of the widths of the gas-filled gaps. However, the diameter of the gas-filled hollow is chosen with the shortest overall heat loss and optimal efficiency in order to increase exergy efficiency and reduce destruction exergy. A solar collector with a gas-filled vacuum between the double-glazing and the absorber (PV model) and the inside glass is also considered in this work, as is a new approach based on the energy and exergy properties of this assembly.

2. METHODOLOGY AND THEORETICAL ANALYSIS

In this work, we have chosen to apply our approach on the PV-T arrangement shown below Figure 1. To find the temperatures and pass the heat transfer coefficients, an iterative approach is used. In addition to being quantitatively investigated, the impacts of Six gases on useful energy, overall heat coefficients, and exit temperature are contrasted. The " $d = d_1 = d_2$" gaps (which range from 2 to 25 mm) are taken to be equal and optimized in order to minimize heat loss and, as a result, maximize useful energy.

- The electrical analogy is used to establish heat transfer coefficients.
- Conditions of quasi-steady-state govern the system's operation.
- Flow direction is the sole determinant of air temperature.
- The flow of air is perpendicular to the cross-sectional plane.
- Radiant energy cannot be absorbed by the fluid.
- Energy radiation is absorbed by glass surfaces.

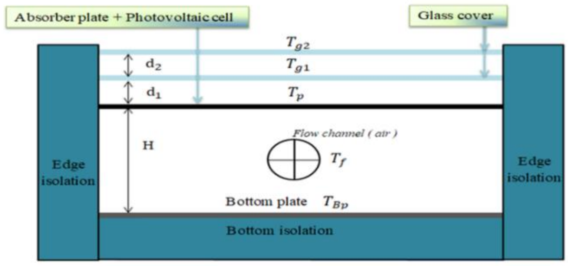

Figure 1. Cross section of the Photovoltaic-Thermal hybrid panel with a rectangular duct

2.1 Energy balance equations

The temperature of each collector component is presented in Figure 1. T_{g2} is the temperature of the top surface of glass 2. T_{g1} The other temperatures are of inner surface of glass 1 and the gas between them. placing the absorbent plate T_p beneath the inner glass cover and separating them with a gas layer, between the T_p absorber and the upper side of the bottom plate T_{Bp} , the fluid (air) to be heated circulates $T_f\ (i)$ in the PVT collector, which leads to an increase in the heat gain of this fluid. the energy balance equation is applied for each element as follows [5, 24, 48]:

2.1.1 The glass cover 2

$$k_{eq,g1-g2} \cdot (T_{g1} - T_{g2}) + S_2 = (h_{r\,g2-a} + h_w) \cdot (T_{g1} - T_{g2}) \qquad (1)$$

$k_{eq,g1-g2}$ = standing for the double-glass equivalent transfer coefficient $\left(\frac{W}{(K.m^2)}\right)$.

$$k_{eq,g1-g2} = \left[\left({}^{e_{g1}}/_{K_{g1}}\right) + \left({}^{e_{g2}}/_{K_{g2}}\right) + \left(h_{c\,g1-g2} + h_{r\,g1-g2}\right)\right]^{-1}$$

S_2 = The energy that glass cover 2 absorbs$\left(\frac{W}{(m^2)}\right)$, which is stated as:

$$S_2 = \alpha_{g2}\,.\,S$$

2.1.2 The glass cover 1

$$(h_{r,p-g1} + h_{c,p-g1}) \cdot (T_p - T_{g1}) + S_1 = U_{g1-a} \cdot (T_{g1} - T_a) \quad (2)$$

S_1 = The energy that glass cover 1 absorbs $\left(\frac{W}{(m^2)}\right)$, which is stated as:

U_{g1-a} = The heat transfer coefficient $\left(\frac{W}{(K.m^2)}\right)$ between glass cover 1 and the ambient.

$$S_1 = \alpha_{g1}.\tau_{g2}\,.\,S$$

$$U_{g1-a} = \left[\left(h_{c\,g2-a} + h_{r\,g2-a}\right)^{-1} + \left({}^{e_{g1}}/_{K_{g1}}\right) + \left({}^{e_{g2}}/_{K_{g2}}\right) + \left(h_{c\,g2-g1} + h_{r\,g2-g1}\right)^{-1}\right]^{-1}$$

2.1.3 The absorber (PV module)

This is the sum of all solar energy that reaches the absorber plate minus the amount of energy that is transformed into electrical energy, denoted as S_p:

$$S_p = h_{c\,p-f} \cdot \left(T_p - T_f\right) + (h_{r,p-g1} + h_{c,p-g1}) \cdot (T_p - T_{g1}) + h_{r,p-Bp} \cdot (T_p - T_{Bp}) \quad (3)$$

Or,

$$S_p = h_{c\,p-f} \cdot \left(T_p - T_f\right) + U_T \cdot (T_p - T_a) + h_{r,p-Bp} \cdot (T_p - T_{Bp}) \quad (4)$$

U_T = the top heat loss coefficient $\left(\frac{W}{(K.m^2)}\right)$ between the absorber and the ambient.

$$U_T = \left[\left(h_{c\,g2-a} + h_{r\,g2-a}\right)^{-1} + \left({}^{e_{g1}}/_{K_{g1}}\right) + \left({}^{e_{g2}}/_{K_{g2}}\right) + \left(h_{c\,g2-g1} + h_{r\,g2-g1}\right)^{-1} + \left(h_{c\,p-g1} + h_{r\,p-g1}\right)^{-1}\right]^{-1}$$

where,

$$S_p = \tau_{g1}\,.\,\tau_{g2}.\tau_{pO}\,S\left[\alpha_p(1-F) + \alpha_{pv}.F\left(1-\eta_{pv}\right)\right] \quad (5)$$

η_{Pv} this is how the PV module's electrical efficiency is determined [49-52]:

$$\eta_{Pv} = \eta_{rf}\left(1 - \beta_{rf}\left(T_p - T_{rf}\right)\right) \quad (6)$$

where, η_{rf} is the reference electrical efficiency at standard conditions (S = 1000 ${}^{W}/_{m^2}$ and T_{rf} = 298.15 K) [53]. The temperature coefficient is assumed as β_{rf} = 0.0041 K^{-1} for crystalline silicon modules [54].

Eqs. (5) and (6) can be combined to give the equation:

$$S_p = \tau_{g1}\,.\,\tau_{g2}.\tau_{pO}\,S\left[\alpha_p(1-F) + \alpha_{pv}.F\left(1 - \eta_{rf}\left(1 - \beta_{rf}\left(T_p - T_{rf}\right)\right)\right)\right] \quad (7)$$

2.1.4 A working fluid's steady-state energy equilibrium equation [55, 56]

$$\frac{\dot{m}.C_f}{W}\frac{dT_f}{dx} = h_{c\,Bp-f}\left(T_{Bp} - T_f\right) + h_{c\,p-f}\left(T_p - T_f\right) \quad (8)$$

The coefficients of heat loss for the absorber plate in relation to both air and the bottom plate.

$$U_{p-f} = \left[\frac{1}{h_{c\,p-f}} + \frac{e_p}{K_p} + \frac{A_e\,e_i}{A_c\,K_{ins}}\right]^{-1}$$

$$U_{p-Bp} = \left[\frac{1}{h_{r\,p-Bp}} + \frac{e_p}{K_p}\right]^{-1}$$

2.1.5 The bottom plate

$$h_{r,p-Bp} \cdot \left(T_p - T_{Bp}\right) = h_{c\,Bp-f} \cdot \left(T_{Bp} - T_f\right) + U_b \cdot \left(T_{Bp} - T_a\right) \quad (9)$$

$$U_b = \left[\frac{1}{h_w} + \frac{e_{ins}}{K_{ins}} + \frac{A_e\,e_i}{A_c\,K_{ins}}\right]^{-1}$$

Finally, Eqs. (3), (8) and (9) can be written $h_{c\,p-f}$ and $h_{r\,p-Bp}$ are substituted by U_{p-f} and U_{p-Bp}, respectively.

$$U_{p-f} \cdot \left(T_p - T_f\right) + \left(h_{r,p-g1} + h_{c,p-g1}\right) \cdot \left(T_p - T_{g1}\right) + U_{p-Bp} \cdot \left(T_p - T_{Bp}\right) = S_p \quad (10)$$

$$U_{p-Bp} \cdot (T_p - T_{Bp}) = h_{c\,Bp-f} \cdot \left(T_{Bp} - T_f\right) + U_b \cdot \left(T_{Bp} - T_a\right) \quad (11)$$

$$\frac{\dot{m}_f.C_f}{W}\frac{dT_f}{dx} = h_{c\,Bp-f}\left(T_{Bp} - T_f\right) + U_{p-f}\left(T_p - T_f\right) \quad (12)$$

By combining and arranging Eqs. (10) and (12):

$$\left(T_p - T_f\right) = S_p\,.\,x_1 - y_1\left(T_f - T_a\right) \quad (13)$$

$$\left(T_{Bp} - T_f\right) = S_p\,.\,x_2 - y_2\left(T_f - T_a\right) \quad (14)$$

The coefficients are x_1, x_2 and y_1, y_2:

$$x_1 = \frac{\left(U_{p-Bp} + U_b + h_{c\,Bp-f}\right)}{\left[\left(U_{p-f} + U_T + U_{p-Bp}\right)\left(U_{p-Bp} + U_b + h_{c\,Bp-f}\right) - U_{p-Bp}{}^2\right]} \quad (15)$$

$$y_1 = \frac{U_T\left(U_{p-Bp} + U_b + h_{c\,Bp-f}\right) + U_{p-Bp}U_b}{\left[\left(U_{p-f} + U_T + U_{p-Bp}\right)\left(U_{p-Bp} + U_b + h_{c\,Bp-f}\right) - U_{p-Bp}{}^2\right]} \quad (16)$$

$$x_2 = \frac{U_{p-Bp}}{\left[\left(U_{p-f} + U_T + U_{p-Bp}\right)\left(U_{p-Bp} + U_b + h_{c\,Bp-f}\right) - U_{p-Bp}{}^2\right]} \quad (17)$$

$$y_2 = \frac{w}{\left[\left(U_{p-f} + U_T + U_{p-Bp}\right)\left(U_{p-Bp} + U_b + h_{c\,Bp-f}\right) - U_{p-Bp}{}^2\right]} \quad (18)$$

$$w = (U_{p-f} + U_T + U_{p-Bp})(U_{p-Bp} + U_b + h_{c\,Bp-f}) + U_T U_{p-Bp} - (U_{p-f} + U_T + U_{p-Bp})(U_{p-Bp} + h_{c\,Bp-f})$$

Substituting Eqs. (13), (14) with Eq. (12) can be written

$$\frac{\dot{m}_f . C_f}{W}\frac{dT_f}{dx} = S_p(x_2 . h_{c\,Bp-f} - x_1 . U_{p-f}) + (y_2 . h_{c\,Bp-f} - y_1\, U_{p-f})(T_f - T_a) \quad (19)$$

If:

$$A = (x_2 . h_{c\,Bp-f} - x_1 . U_{p-f}) \quad (20)$$

$$B = (y_2 . h_{c\,Bp-f} - y_1\, U_{p-f}) \quad (21)$$

(19) becomes:

$$\frac{\dot{m}_f . C_f}{W}\frac{dT_f}{dx} = \frac{d\emptyset_u}{dA_c} = A.S_p - B\,(T_f - T_a) \quad (22)$$

$$\frac{d\emptyset_u}{dA_c} = A.\left(S_p - \frac{B}{A}(T_f - T_a)\right) = F' .\left(S_p - U_L\,(T_f - T_a)\right) \quad (23)$$

where, $F' = A$ and $U_L = \frac{B}{A}$.

Ultimately, we get the following after solving this final equation and applying the boundary conditions:

This is the useful heat energy of the considered FPPV-T [57, 58]:

$$\emptyset_u = A_c\, F_R\,\left(S_p - U_L\,(T_{fi} - T_a)\right) \quad (24)$$

$$F_R = \frac{\dot{m}_f . C_f}{A_c . U_L}\left(1 - exp\left(-\frac{F' . A_c . U_L}{\dot{m}_f . C_f}\right)\right) \quad (25)$$

By discretizing the working fluid equation using the Crank-Nicolson technique, we get (12) as a solution.

$$\frac{T_f(i+1) - T_f(i)}{\Delta x} = \frac{W}{\dot{m}_f . C_f}(h_{c\,Bp-f} T_{Bp} + U_{p-f}\, T_p) - \frac{1}{2}\frac{W}{\dot{m}_f . C_f}(h_{c\,Bp-f} + U_{p-f})(T_f(i+1) + T_f(i)) \quad (26)$$

Eqs. (1)-(2)-(10) and (11) and (26) can be expressed as a 5 × 5 matrix ($[a][T] = [b]$), as follows:

$$\begin{bmatrix} a_1 & a_2 & 0 & 0 & 0 \\ 0 & a_3 & a_4 & 0 & 0 \\ 0 & a_5 & a_6 & a_7 & a_8 \\ 0 & 0 & a_9 & a_{10} & a_{11} \\ 0 & 0 & a_{12} & a_{13} & a_{14} \end{bmatrix}\begin{bmatrix} T_{g2} \\ T_{g1} \\ T_p \\ T_{Bp} \\ T_f(i+1) \end{bmatrix} = \begin{bmatrix} b_1 \\ b_2 \\ b_3 \\ b_4 \\ b_5 \end{bmatrix} \quad (27)$$

where:

$$a_1 = (k_{eq,g1-g2} + h_{r\,g2-a} + h_w)$$

$$a_2 = -k_{eq,g1-g2}$$

$$a_3 = (h_{r,p-g1} + h_{c,p-g1} + U_{g1-a})$$

$$a_4 = -(h_{r,p-g1} + h_{c,p-g1})$$

$$a_5 = -(h_{r,p-g1} + h_{c,p-g1})$$

$$a_6 = (h_{r,p-g1} + h_{c,p-g1} + h_{c,p-f} + U_{p-Bp})$$

$$a_7 = -U_{p-Bp}$$

$$a_8 = -h_{c,p-f}$$

$$a_9 = U_{p-Bp}$$

$$a_{10} = -(U_{p-Bp} + U_p + h_{c,Bp-f})$$

$$a_{11} = h_{c,Bp-f}$$

$$a_{12} = \frac{\Delta x . W}{\dot{m}_f . C_f} U_{p-f}$$

$$a_{13} = \frac{\Delta x . W}{\dot{m}_f . C_f} h_{c\,Bp-f}$$

$$a_{14} = -\left(1 + \frac{\Delta x . W}{2 . \dot{m}_f . C_f}(h_{c\,Bp-f} + U_{p-f})\right)$$

$$b_1 = S_2 + (h_{r\,g2-a} + h_w)\cdot T_a$$

$$b_2 = S_1 + U_{g1-a}\cdot T_a$$

$$b_3 = S_p$$

$$b_4 = -U_p \cdot T_a$$

$$b_5 = \left(\frac{\Delta x . W}{2 . \dot{m}_f . C_f}(h_{c\,Bp-f} + U_{p-f}) - 1\right) . T_f(i)$$

2.2 Natural convection and radiative coefficients related to the glass cover g2

In Eq. (28) and Eq. (29) we applied the following formulas $(h_w = h_{c\,g2-a})$ for the natural convection that happens when the wind moves across glass cover 2 to the atmosphere [55, 59, 60].

$$hw = 3.0 \cdot V_w + 2.8 \qquad V_w \le 5\ m/s \quad (28)$$

$$hw = 6.15 \cdot V_w^{0.8} \qquad V_w > 5\ m/s \quad (29)$$

The coefficient of radiative heat loss to sky:

$$h_{r\,g2-a} = \sigma . \varepsilon_{g2} . \frac{(T_{g2}^4 - T_s^4)}{(T_{g2} - T_a)} \quad (30)$$

T_s = Sky temperature (K). The empirical relation is used to calculate it [57, 61]:

$$T_s = T_a \left(0.711 + 0.0056T_{dp} + 0.000073T_{dp}^2 + 0.013\ \cos(15t)\right)^{0.25} \quad (31)$$

$$0\ °C < T_{dp} < 93°C$$

$$T_{dp} = 6.54 + 14.526\ln(p_w) + 0.7389\ln(p_w)^2 + 0.09486\ln(p_w)^3 + 0.4569(p_w)^{0.1984} \quad (32)$$

T_{dp} = the dew-point temperature (K) can be calculated directly by one of the following equations [62]:

$$T_{dp} < 0\ °C$$

$$T_{dp} = 6.09 + 12.60\ ln(p_w) + 0.4959\ ln(p_w)^2 \quad (33)$$

$$RH = 100.\phi \text{ And: } \phi = {}^{p_w}/_{p_{sw}}$$

p_{sw}= the atmospheric pressure at which vaporization occurs (in pascal) [63]:

for $T > 0\ °C$

$$p_{sw}(T) = 0.61121.\exp\left(\left(18.678 - \frac{T}{234.5}\right)\left(\frac{T}{257.14 + T}\right)\right) \quad (34)$$

for $T < 0\ °C$

$$p_{sw}(T) = 0.61115.\exp\left(\left(23.036 - \frac{T}{233.7}\right)\left(\frac{T}{279.82 + T}\right)\right) \quad (35)$$

2.3 Natural convection coefficients in the double-glazing and between the inner glass cover and the absorber

The coefficients of radiative heat transfer between the two layers of glass, the selective absorber and the inner glass cover, the absorber and the bottom plate are, respectively.

$$h_{r\ g2-g1} = \sigma.\frac{(T_{g1} + T_{g2})(T_{g1}{}^2 + T_{g2}{}^2)}{(\frac{1}{\varepsilon_{g1}} + \frac{1}{\varepsilon_{g2}} - 1)} \quad (36)$$

$$h_{r\ g1-p} = \sigma.\frac{(T_{g1}+T_p)(T_{g1}{}^2+T_p{}^2)}{(\frac{1}{\varepsilon_{g1}}+\frac{1}{\varepsilon_p}-1)} \quad (37)$$

$$\mathbf{h}_{r\ p-Bp} = \boldsymbol{\sigma}.\frac{(\mathbf{T_p} + \mathbf{T}_{Bp})(\mathbf{T_p}^2 + \mathbf{T_{Bp}}^2)}{(\frac{\mathbf{1}}{\boldsymbol{\varepsilon}_p} + \frac{\mathbf{1}}{\boldsymbol{\varepsilon}_{Bp}} - \mathbf{1})} \quad (38)$$

2.4 Natural convection coefficients in the double-glazing and between the inner glass cover and the absorber

The air in the gap between the plates is intended to be replaced by gases such as Argon, Krypton, Xenon, Carbon monoxide and Sulfur dioxide. The temperature that manifests at a distance x from the PV-T entry determines their thermo-physical characteristics.

ρ_{gaz} the density of every gas is calculated by the formula:

$$\boldsymbol{\rho_{gaz}} = (\boldsymbol{P_a}.\boldsymbol{M_m})/(\boldsymbol{Z}.\boldsymbol{R}.\boldsymbol{T_m}) \quad (39)$$

2.4.1 Thermo-physical

The following polynomials can be used to compute thermal and transport properties [43, 64, 65].

The Air

$$K_{air} = (0.0965.\ T_m - 9.960.10^{-6}.\ T_m^2 - 9.310.10^{-8}.\ T_m^3 + 8.882.10^{-11}.\ T_m^4\ ).10^{-3} \quad (40)$$

$$\rho_{air} = (0.02897 * P_a)/(0.9997 * 8.314 * T_m) \quad (41)$$

$$C_{p\ air} = 1047.63657 - 0.372589265.\ T_m + 9.4530421.10^{-4}.\ T_m^2 - 6.02409443.10^{-7}.\ T_m^3 + 1.2858961.10^{-10}.\ T_m^4 \quad (42)$$

$$\mu_{air} = 7.72488.10^{-8}.\ T_m - 5.95238.10^{-11}.\ T_m^2 + 2.71368.10^{-14}.\ T_m^3 \quad (43)$$

The Argon gas

$$K_{Ar} = (0.0606\ T_m + 3.151.10^{-5}.\ T_m^2 - 1.525.10^{-7}.\ T_m^3 + 1.223.10^{-10}.T_m^4\ ).10^{-3} \quad (44)$$

$$\rho_{Ar} = P_a/(0.99937 * 209.17 * T_m) \quad (45)$$

$$C_{p\ Ar} = 521.55\ J/(Kg.K) \quad (46)$$

$$\mu_{Ar} = 7.91722.10^{-8}.\ T_m + 2.93448.10^{-11}.\ T_m^2 - 1.73227.10^{-13}.\ T_m^3 + 1.41721.10^{-16}.\ T_m^4 \quad (47)$$

The Krypton gas

$$K_{Kr} = (0.327\ T_m + 1.632.10^{-6}.\ T_m^2 - 2.060.10^{-8}.\ T_m^3 + 1.042.10^{-11}.T_m^4\ ).10^{-3} \quad (48)$$

$$\rho_{Kr} = P_a/(0.99793 * 100.18 * T_m) \quad (49)$$

$$C_{p\ Kr} = 249.2\ J/(Kg.K) \quad (50)$$

$$\mu_{Kr} = 8.56676.10^{-8}.T_m + 1.91155.10^{-11}.T_m^2 - 1.05643.10^{-13}.T_m^3 + 1.09675.10^{-16}.T_m^4 \quad (51)$$

The Xenon gas

$$K_{Xe} = (0.0209\ T_m - 1.629.10^{-5}.T_m^2 + 3.703.10^{-8}.T_m^3 - 3.322.10^{-11}.T_m^4).10^{-3} \quad (52)$$

$$\rho_{Xe} = P_a/(0.99471 * 64.645 * T_m) \quad (53)$$

$$C_{p\ Xe} = 160.09\ J/(Kg.K) \quad (54)$$

$$\mu_{Xe} = 7.33337.10^{-8}.\ T_m + 3.93839.10^{-11}.T_m^2 - 1.05562.10^{-13}.T_m^3 + 6.29110.10^{-17}.T_m^4 \quad (55)$$

The Carbon Monoxide gas

$$K_{CO2} = (0.0872\ T_m + 1.659.10^{-6}.T_m^2 - 6.481.10^{-8}.T_m^3 + 5.244.10^{-11}.T_m^4).10^{-3} \quad (56)$$

$$\rho_{CO2} = P_a/(0.99964 * 298.4 * T_m) \quad (57)$$

$$C_{p\ CO2} = 1042.1\ J/(Kg.K) \quad (58)$$

$$\mu_{CO2} = 7.11110.10^{-8}.\ T_m - 2.80674\ .10^{-11}.T_m^2 - 5.36367.10^{-14}.T_m^3 + 6.27741.10^{-17}.T_m^4 \quad (59)$$

The Sulfur dioxide

$$K_{Ne} = (0.0475T_m - 1.622\ .10^{-4}.T_m^2 + 4.816.10^{-7}.T_m^3 - 3.747\ .10^{-10}.T_m^4).10^{-3} \quad (60)$$

$$\rho_{Ne} = P_a/(0.98285 * 143.74 * T_m) \quad (61)$$

$$C_{pNe} = 656.2\ J/(Kg.K) \quad (62)$$

$$\mu_{Ne} = 5.28546.10^{-8}.T_m - 1.02879.10^{-10}.T_m^2 + 3.28719.10^{-13}.T_m^3 - 3.21789.10^{-16}.T_m^4 \quad (63)$$

The formula determines the average temperature T_m at local point (i) for the two glass covers and the inner glass cover with the absorber (PV module).

$$T_m(i) = \frac{T_{g1}(i) + T_{g2}(i)}{2} \quad (64)$$

$$T_m(i) = \frac{T_{g1}(i) + T_p(i)}{2} \quad (65)$$

2.4.2 Natural convection in the filled-gas space and coefficients calculation

By calculating the Nusselt number and Rayleigh number provided by Eismann, we can assess the convective heat loss across the gap between the both panes of glass and the inside glass-cover and the absorber (PV module) which vary from 2 mm to 25 mm.

$$Ra'_{g1-g2} = \frac{g.\beta'.d^3.(T_{g1}-T_{g2})}{\upsilon_{gaz}.\alpha_{D\ gas}} cos(\beta) = Ra\ cos(\beta) \quad (66)$$

And,

$$Ra'_{g1-p} = \frac{g.\beta'.d^3.(T_p - T_{g1})}{\upsilon_{gaz}.\alpha_{D\ gas}} cos(\beta) = Ra\ cos(\beta) \quad (67)$$

$$\beta' = {}^{1}/_{T_m},\ \alpha_{D\ gas} = {}^{K\ gaz}/_{(C_{p\ gas}.\rho_{\ gaz})},\ \upsilon_{gaz} = {}^{\mu\ gaz}/_{\rho\ gaz}$$

The Hollands correlation [17] is used by a majority of researchers to anticipate the heat transfer coefficient in situations of natural convection. However, Eismann [19] has created an enhanced and more precise equation, which is being utilized in the current study. The formulation he derived is presented below:

$$Nu = Nu_{cond} + Nu_{CONV\ I} + Nu_{CONV\ II} \quad (68)$$

$$\mathrm{Nu_{cond}} = 1 \quad (69)$$

$$Nu_{CONV\ I} = 1.44\left(1 - \frac{1708}{Ra' + 1708\ Rc}\right)\left(1 - \frac{1708(sin(1.8\ \beta))^{1.6}}{Ra' + 1708\ Rc}\right) \quad (70)$$

$$\mathrm{Nu_{CONV\ II}} = \left(\left(\frac{Ra' + 5830\ Rc}{5830}\right)^{0.39} - 1\right)(1 + C.Rc) \quad (71)$$

$C = 0.29$.

Rc = 0 is first iteration's starting value was taken into account. Upon completion of the initial cycle, the value is initialized to:

$$\mathrm{Rc} = \exp\left(-\frac{A_C.F'.U_L}{\dot{m}_f.C_p}\right)$$

Following are the estimated values of the heat transfer coefficients between the two panes of glass and between the inside of the glass and absorber:

$$h_{c\ g1-g2} = \frac{Nu_{g1-g2} + K_{gaz}}{d} \quad (72)$$

$$\mathrm{h_{c\ g1-p}} = \frac{\mathrm{Nu_{g1-p} + K_{gaz}}}{d} \quad (73)$$

2.5 Forced convection heat transfer coefficients

By analyzing the flow regime, one may determine the forced convection heat transfer coefficients between the plate bottom and airflow, and between the selective absorber (PV module) and airflow.

2.5.1 Laminar flow in an air duct causes forced convection. is modeled using the following correlations [66]

$$\mathrm{Nu} = 8.235\left[1 - 2.0421\left(\frac{\mathrm{H}}{W}\right) + 3.0853\left(\frac{\mathrm{H}}{W}\right)^2 - 2.4765\left(\frac{\mathrm{H}}{W}\right)^3 + 1.0578\left(\frac{\mathrm{H}}{W}\right)^4 - 0.1861\left(\frac{\mathrm{H}}{W}\right)^5\right] \quad (74)$$

The following equation is to approximate the friction factor:

$$\mathcal{F} = 24\left[1 - 1.3553\left(\frac{\mathrm{H}}{W}\right) + 1.9467\left(\frac{\mathrm{H}}{W}\right)^2 - 1.7012\left(\frac{\mathrm{H}}{W}\right)^3 + 0.9564\left(\frac{\mathrm{H}}{W}\right)^4 - 0.2537\left(\frac{\mathrm{H}}{W}\right)^5\right] \quad (75)$$

2.5.2 Turbulent flow in an air duct causes forced convection. is modeled using the following correlations [67, 68]:

$$\mathrm{Nu} = \frac{\left(\frac{\mathcal{F}}{8}\right)(Re - 1000).Pr}{1.07 + 12.7\left(\frac{\mathcal{F}}{8}\right)^{0.5} Pr^{2/3} - 1} \quad (76)$$

For, $0.5 < Pr \leq 2000$ and $4000 < Re \leq 5 \times 10^6$.

Considering the relative roughness (r/D_h), the friction factor is given by:

$$\mathcal{F} = \left[-2.\log_{10}\left(\frac{2r}{7.54\,D_h} - \frac{5.02}{Re}\log_{10}\left(\frac{2r}{7.54\,D_h} + \frac{13}{Re}\right)\right)\right]^{-2} \quad (77)$$

For, $4000 < Re \leq 10^8$ and $2.10^{-8} < (r/D_h) \leq 0.1$.

Here are the heat transfer coefficients in the region of the airflow and the absorber (PV module) and, the region of the bottom plate and the flowing air, respectively.

$$\mathrm{h}_{c\,p-f} = \frac{Nu_{p-f}\,.K_{air}}{D_h} \quad (78)$$

$$\mathrm{h}_{c\,Bp-f} = \frac{Nu_{Bp-f}\,.K_{air}}{D_h} \quad (79)$$

2.6 Energy study

The PV/T air collectors are evaluated thermo-hydraulic and electrically based on a number of parameters, including effective thermal efficiency, pressure loss, power consumption by fans, and power generation by electrical means. The ratio of the total incident solar radiation to the heat benefit less the equivalent fan power is known as the effective thermal efficiency (η_{th}), and it can be expressed as follows:

$$\eta_{th} = \frac{\emptyset_u - P_f}{(S.A_c)} \quad (80)$$

$\emptyset_u$ the useful heat collected is given by Eq. (24).

The equivalent electrical efficiency of PV panel (η_{EPV}) is estimated as:

$$\eta_{\mathrm{EPv}} = \frac{\eta_{\mathrm{Pv}}}{C_f} \quad (81)$$

η_{Pv} the electrical efficiency of the PV module is calculated in Eq. (6).

C_f is the conversion factor of the thermal power plant (in the range 0.29-0.4 [50-52, 69]), and assumed equal to 0.36.

The total combined FPPV-T collector (hybrid) efficiency (η_{C}) is obtained as follows [51, 69]:

$$\eta_{\mathrm{C}} = \eta_{th} + \eta_{\mathrm{EPv}} \quad (82)$$

2.7 Exergy study

Energy analysis is helpful in figuring out how well PV/T collectors work, how energy degrades during thermal and electrical conversion processes, and how to design and run PV/Ts to use energy as efficiently as possible.

The exergy analysis is conducted by considering the total exergy input, exergy outflow, and exergy destroyed from the system, in accordance with the principles of the second law of thermodynamics. The exergy efficiency of the FPPV-T air heater can be determined by calculating the ratio of the desired output exergy, known as product exergy, to the exergy inflow. Exergy is a measure of the energy's quality. The optimal spacing between the FPPV-T plates can be determined using an alternative approach that considers both the maximum exergy and the exergy efficiency. This method is used to verify the gaps identified by graphical analysis of maximum energy efficiency and usable energies.

The application of the exergy balance equation to the FPPV-T results in [58, 70-72]:

$$\sum \dot{E}_{int} - \sum \dot{E}_{out} = \sum \dot{E}_{des} \quad (83)$$

Or,

$$\dot{E}_{des} = \dot{E}_{sun} - \left(\dot{E}_{air\,out} - \dot{E}_{air\,int}\right) - \dot{E}_{pv} - \dot{E}_{fan} \quad (84)$$

The following represents the input exergy that solar radiation supplies which reaches the PV/T collector surface [32, 73]:

$$\dot{E}_{sun} = S_p\,A_c\left[1 - \frac{4}{3}\left(\frac{T_a}{T_{sun}}\right) + \frac{1}{3}\left(\frac{T_a}{T_{sun}}\right)^4\right] \quad (85)$$

The solar surface temperature is regarded as a significant contributor to exergy $T_{sun} = 5770\,K$.

The fan's exergy is quantified by:

$$\dot{E}_{fan} = \frac{T_a}{T_{int}} P_{fan} \quad (86)$$

And, $P_{fan} = \frac{\dot{m}_f.\Delta p}{\rho_{air}.\eta_{fan}.\eta_{mot}}$.

The thermal exergy:

$$\dot{\boldsymbol{E}}_{\boldsymbol{th}} = \dot{\boldsymbol{E}}_{\boldsymbol{air\,out}} - \dot{\boldsymbol{E}}_{\boldsymbol{air\,int}} \quad (87)$$

Or,

$$\dot{E}_{th} = \dot{m}_f.\left[(h_{air\,out} - h_{air\,int}) - T_a\,(S_{air\,out} - S_{air\,int})\right] \quad (88)$$

The variables h and S represent the enthalpy and entropy of air, respectively, as well as the enthalpy and entropy differential between the inlet and output air masses.

$$\dot{E}_{th} = \emptyset_u - \dot{m}_f\,.T_a\left(\mathrm{C}_p \ln\left(\frac{T_{out}}{T_{int}}\right) - \mathrm{R}_{air}\ln\left(\frac{p_{out}}{p_{int}}\right)\right) \quad (89)$$

The electrical exergy [74]:

$$\dot{E}_{pv} = \eta_{\mathrm{Pv}}\,\mathrm{A}_c\,\mathrm{S} \quad (90)$$

The photovoltaic thermal (PV-T) exergy:

$$\dot{E}_{PV-T} = \dot{E}_{th} + \dot{E}_{pv} \tag{91}$$

According to Eq. (84), exergy destruction refers to the portion of solar radiation exergy that is not utilized by the system, in addition to the electrical and thermal exergy production. Therefore, it is represented as:

$$\dot{E}_{des} = \mathrm{S}_p\ \mathrm{A}_c\left[1-\frac{4}{3}\left(\frac{T_a}{T_{sun}}\right)+\frac{1}{3}\left(\frac{T_a}{T_{sun}}\right)^4\right]-\dot{E}_{PV-T} - \left(\frac{T_a}{T_{int}}\frac{\dot{m}_f.\Delta p}{\rho_{air}\ .\eta_{fan}.\eta_{mot}}\right) \tag{92}$$

The exergy efficiency of the flat plate photovoltaic-thermal (FPPV-T) can be determined for the specific gaseous systems being investigated [71, 73-75].

$$\eta_{ex} = \frac{\dot{E}_{out}}{\dot{E}_{int}} = \frac{\dot{E}_{PV-T}\ +\left(\frac{T_a}{T_{int}}\frac{\dot{m}_f.\Delta p}{\rho_{air}\ .\eta_{fan}.\eta_{mot}}\right)}{\mathrm{S}_p\ \mathrm{A}_c\left[1-\frac{4}{3}\left(\frac{T_a}{T_{sun}}\right)+\frac{1}{3}\left(\frac{T_a}{T_{sun}}\right)^4\right]} \tag{93}$$

3. NUMERICAL CALCULATIONS

Iterations and matrix inversion are used to solve the system of Eq. (27) and determine the temperature. The system's solution is iterated until each point (i.Δx) experiences convergence. The following step then makes use of the collected temperatures which are then applied in another step. the calculation of heat transfer coefficients is performed. with these temperatures at each interval until the total length of the photovoltaic thermal hybrid panel is reached. the heat transfer coefficients, Nusselt numbers, and overall heat loss coefficients at each location along the PV-T are calculated. For every parameter, an average is calculated.

The photovoltaic thermal hybrid panel PV-T air reaches its outlet temperatures when converg-ence takes place and the last point is calculated.

The average heat transfer coefficients:

$$\overline{h_{c\,g1-g2}} = \frac{1}{N}\sum_{i=1}^{N} h_{c\,g1-g2}(i) \tag{94}$$

$$\overline{h_{c\,p-g1}} = \frac{1}{N}\sum_{i=1}^{N} h_{c\,p-g1}(i) \tag{95}$$

The average local Nusselt numbers:

$$\overline{Nu_{g1-g2}} = \frac{1}{N}\sum_{i=1}^{N} Nu_{g1-g2}(i) \tag{96}$$

$$\overline{Nu_{p-g1}} = \frac{1}{N}\sum_{i=1}^{N} Nu_{p-g1}(i) \tag{97}$$

The average overall heat loss coefficients:

$$\overline{U_L} = \frac{1}{N}\sum_{i=1}^{N} U_L(i) \tag{98}$$

With, $N = \frac{L}{\Delta x}$.

The temperature is a term that resolves all the unknowns of the photovoltaic thermal panel are reached when the calculation of the last point is performed and when convergence occurs T_f.or this enables the determination of a novel value for the fluid temperature of the last point $\left(T_f(i+1)\right)$ to be obtained, which is compared to the value estimated at the beginning$\left(T_f(i)\right)$. Eventually, T_f is obtained by an iterative process. This assignment is Applied to the five mentioned gases. Then the useful heat energy and the effective thermal efficiency, the equivalent electrical efficiency of PV panel, and the total combined FPPV-T collector (hybrid) efficiency calculated by Eqs. (24) and (80), (81) and (82) respectively.

The photovoltaic thermal (PV-T) exergy, destruction exergy and the exergy efficiency addition-ally employed as a means of validating a PV-T hybrid panel's ideal filled gas gaps.

The inputs for the simulation model, after setting the rest of PVT panel parameters (Table 1), are the following: radiation S, ambient temperature T_a, wind speed V_w wind, tilt angle β and mass flow $\dot{m}_f$.

After establishing the other parameters of the PVT panel (Table 1), the simulation model requires the following inputs: radiation (S), wind speed (V_w), ambient temperature (T_a), tilt angle (β), and mass flow ($\dot{m}_f$).

Table 1. Important characteristics of the PVT panel that was investigated

Component	Value	Component	Value
L	$15\ m$	α_{pv}	0.044
W	$2\ m$	α_{g1}, α_{g2}	0.044
H	$0.25\ m$	α_p	0.95
β	40	e_{g1}, e_{g2}	0.005
V_w	$5\ m/s$	e_p	0.003
$\dot{m}_f$	$0.7\ Kg/s$	e_i	0.05
$T_{f\ int}$	$295.15\ K$	k_{g1}, k_{g2}	0.7
T_a	$284{,}15\ K$	k_p	207
Φ	0.5	k_i	0.027
τ_{po}	0.88	F	0.628
τ_{g1}, τ_{g2}	0.88	η_{rf}	0.125
ε_{Bp}	0.90	β_{rf}	0.0046
ε_p	0.1	T_{rf}	$298{,}15\ K$
$\varepsilon_{g1}, \varepsilon_{g2}$	0.88	S	1000

4. RESULTS AND DISCUSSION

The procedure of choosing the filling gas is influenced by both the gap (2 mm and 25 mm) and the physical properties of the gas. For this reason, the use of the Eismann correlation [19] replaced the Holland connection because it is thought to be more accurate. It is fresh in this theoretical study, and. because it is impossible to report on performance improvements when a specific gas is separated from its ideal gaps in the photovoltaic thermal hybrid panel. Additionally, the energy analysis employed to compute heat loss through double glazing and absorber (PV model) and ascertain the natural convection characteristics in photovoltaic thermal (PV-T) panels is novel.

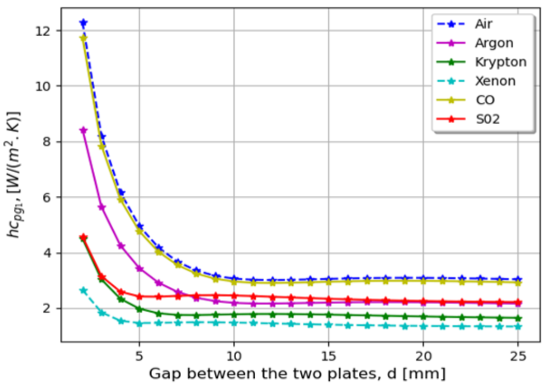

Figure 2. Averaged heat transfer coefficient between inner glass and absorber (PV model)

The confined gases' coefficients of heat transfer (Air, CO, and Argon) between the absorber and the inner glass cover can reach up to ($13\ \mathrm{W.m^{-2}.K^{-1}}$) when the gas-filled region is less than (10mm).however, when the gas-filled region is less than (6 mm), the heat transfer coefficients of the other gases (sulfur dioxide, Krypton, and Xenon) are up to ($5\ \mathrm{W.m^{-2}.K^{-1}}$) (Figure 2). On the one hand, there is a slight decrease in the heat transfer coefficients of trapped gases in double glazing. The curves for Air and Carbon oxide are very similar. It can range from to ($2.9945\ \mathrm{W.m^{-2}.K^{-1}}$) and ($2.8895\ \mathrm{W.m^{-2}.K^{-1}}$) at (10 mm) and ($2.8921\ \mathrm{W.m^{-2}.K^{-1}}$) , ($2.7871\ \mathrm{W.m^{-2}.K^{-1}}$) at (25mm) ,respectively suggesting that a gap greater than (10mm) has no impact. Additionally, the Argon is a gas with a lower heat transfer coefficient than air and CO It can range from to ($2.1341\ \mathrm{W.m^{-2}.K^{-1}}$) at (10 mm) .and ($2.059\ \mathrm{W.m^{-2}.K^{-1}}$) at (25mm).but the sulfur dioxide can range from to ($2.3444\ \mathrm{W.m^{-2}.K^{-1}}$) at (6 mm) and ($2.0611\ \mathrm{W.m^{-2}.K^{-1}}$) at (25 mm). This is a result of double-glazed windows' improved argon-based heat isolation capabilities. making it appropriate for (PV-T) system. the sulfur dioxide stays better than Argon whose value is somewhat ($1.4162\ \mathrm{W.m^{-2}.K^{-1}}$) at (6 mm) and they're approaching equal value between ($2.1941\ \mathrm{W.m^{-2}.K^{-1}}$) at (16 mm) and ($2.062\ \mathrm{W.m^{-2}.K^{-1}}$) at (25 mm) and can also be enclosed in the gaps to minimize heat loss via the double glass and absorber The Xenon curve indicates that it has a value half that of air. It can range from ($1.4163\ \mathrm{W.m^{-2}.K^{-1}}$) for (6 mm) to ($1.2347\ \mathrm{W.m^{-2}.K^{-1}}$) for (25 mm), so less gas would be required to achieve better insulation in comparison to other gases (Air, Argon, Krypton, SO_2, CO). (Figure 3), as reported in the research of Antonanzas et al. [34] When producing domestic hot water (DHW) or hot water suitable for space heating, the same result in our research, Overall, Argon was identified as the most suitable filling gas considering economic and environmental factors (Figure 4).

The air's overall heat loss coefficients are, $2.7569\ \mathrm{W/(m^2.K)}$ to $2.7395\ \mathrm{W.m^{-2}.K^{-1}}$. It is not comparable to CO. the latter ranges between $2.7104\ \mathrm{W.m^{-2}.K^{-1}}$ to $2.6912\ \mathrm{W.m^{-2}.K^{-1}}$ for the same spaces from (10 mm), to (25 mm), in contrast, Xenon's ranges which are from 1.9889 to $1.9168\ \mathrm{W.m^{-2}.K^{-1}}$(from5, to25 mm). In other words, at (5 mm), the two gases exhibit a difference of $1.5\ \mathrm{W.m^{-2}.K^{-1}}$, but Krypton and Sulfur dioxide has values of 2.2577 and $2.4672\ \mathrm{W.m^{-2}.K^{-1}}$ (Figure 5).

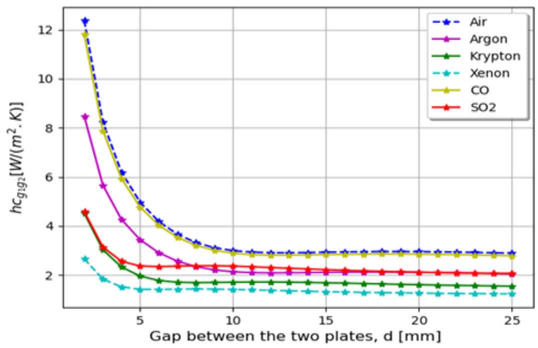

Figure 3. Averaged heat transfer coefficient inside double-glass

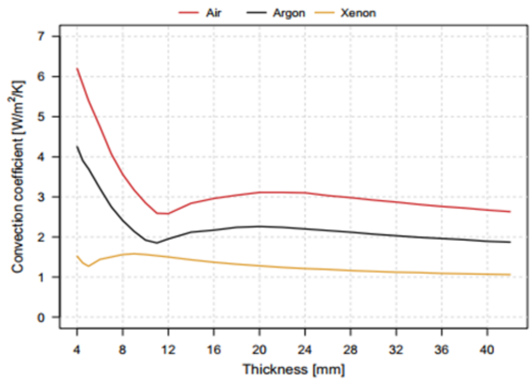

Figure 4. Convective coefficients for different distances between covers and gases [34]

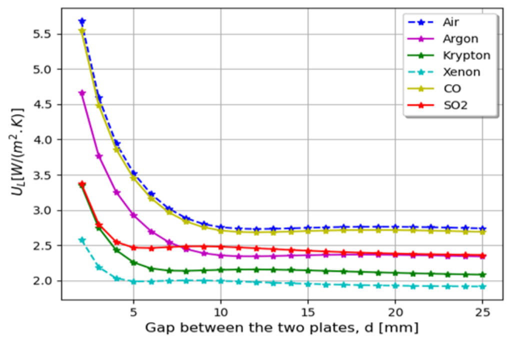

Figure 5. Overall heat loss coefficient of photovoltaic thermal hybrid

When thermal insulation is achieved through fenestration with vertical double-glazing, a U-value is frequently utilized. The fenestration of Chapter 15 displays graphical results from ASHRAE 2017 [62] that exhibit the similar trend as Figure 5. Our mathematical model is validated by the fact that the ideal widths of the gaps filled by Air, Argon and Krypton are practically equal.

Because Xenon produces a lower UL value and the heat transfer coefficients, at 5mm and 25mm, the useful heat energy of PV-T increases to 5.2924 and 5.3698 KW, respectively. However, the useful heat energy by Air is 3.977 *KW* and 4.5793 KW (From 5 to 25 mm), while CO gives 4.027 – 4.621 KW (From 5 to 25 mm). They have almost the same values. When these three gases are compared, it can be shown that the energy obtained differs by approximately $1.3 - 0.72KW$ (From 5 to 10 mm), more useful heat energy is produced by the remaining tested noble gases than by air (Figure 6).

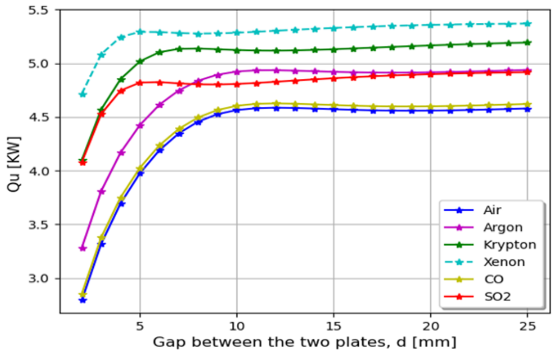

Figure 6. Useful heat energy of PV-T according to the gas utilized

The effect of Gap between for each gas the two plates on the thermal efficiency Where Xenon gas is less valuable and ranges between 0.1764 to 0.179 (From 5 to 25 mm), However, the thermal efficiency by air is 0.1512 at 10 mm, so the Xenon gas offers an advantage of 2%. Still, as the influence of the gap between each gas increases, the thermal efficiency rises as well. Ranging from between 0.15 to 0.18 (From 5 to 25 mm) For all used gases the stability of electrical efficiency in terms of the gap between each of the two plates gas 0.1141, is evidence of its correlation with the absorber's average temperature$\left(\overline{T_p} = \overline{T_{pv}}\right)$ (Figure 7).

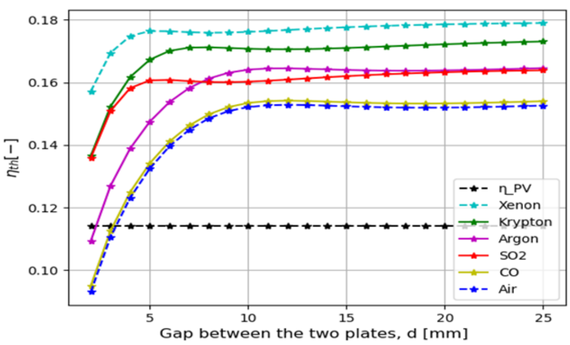

Figure 7. The thermal and electrical efficiency of PV-T

The total combined efficiency is the combination the thermal and equivalent electrical efficiency Eq. (82), for all used gases, the range is 0.47 to 0.50 (From 5 to 25 mm). Nevertheless, total combined efficiency rises in tandem with the influence of the spacing between each gas. The PV-T's overall combined efficiency increases with Xenon noble gas to 0.4935 at 5 mm and to 0.496 at 25 mm, followed closely by Krypton at the same spacing with a value of 0.4843-0.4901. Argon at 25 mm displayed a total efficiency of 0.4816, still showcases competitive performance. on the other hand, gases like sulfur dioxide (SO_2), carbon monoxide (CO), and air exhibit lower total efficiencies, hence the Xenon gas offers a 3% improvement, followed closely by Krypton a 2% and Argen a 1%. Further, these findings underscore the potential for significant total efficiency gains through careful gas selection and spacing optimization. Additionally, the study identifies the suitability of greenhouse dryers for high moisture crops and natural convection for low moisture crops, providing valuable insights for agricultural applications (Figure 8).

The plotted curves in Figure 8 illustrate that the highest efficiency for Argon is attained when there's a 9 mm gas gap between the absorber and double-glazing. This outcome mirrors the findings reported by Vestlund et al. [76]. In their 2012 study, even though their investigation was limited to a solar water heater utilizing double windows. the researchers' findings echoed the consensus that this particular gas filling distance consistently leads to optimal efficiency consistently, highlighting its relevance across diverse research scopes within the realm of solar heating systems (Figure 9).

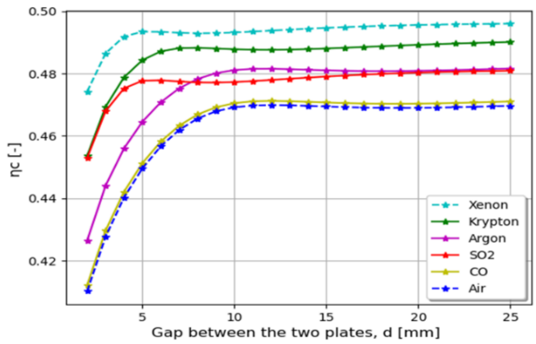

Figure 8. The total combined efficiency of PV-T

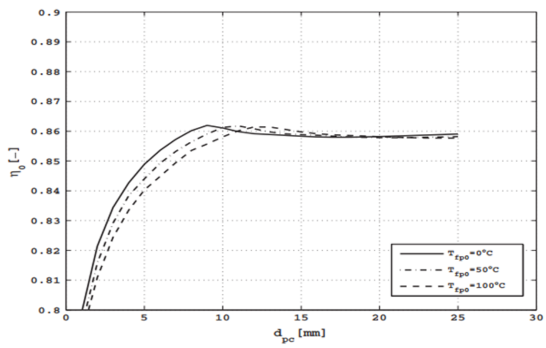

Figure 9. The efficiency of an argon-filled solar collector at Tw = Ta = 25℃ as a function of the distance between the absorber plate and cover glazing with pressure temperatures [76]

For the specific PV-T utilized in our simulation, we observe that the output temperatures for Xenon grow to 302.6634 K at 5 mm, compared to 301.6299 K at 10mm for air. The difference in output temperatures obtained is about 1.02 K.

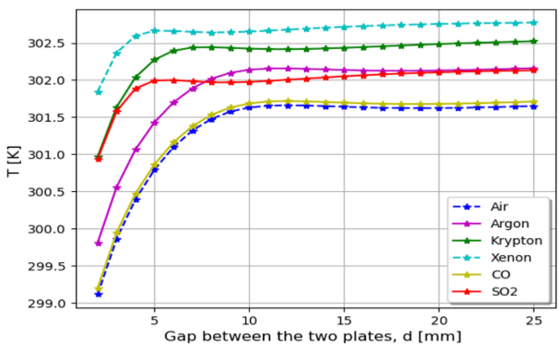

Figure 10. PV-T output temperature delivered depending on the filling gas in the space

The most desirable width of the gas-filled space, which yields the overall heat loss factor and lowest local heat transfer coefficient this is, the most useful heat energy and the total combined efficiency—can be found using the simulation results (Figure 1-Figure 10).

The originality emphasised at the outset stems from employing exergy analysis, encompassing destruction exergy, exergy efficiency, and exergy output, in correlation with gas selection and the gaps between double-glazing and the absorber. Notably, the exergy investigation conducted in this study brings to light that Xenon stands out as a more effective option in reducing exergy destruction compared to other gases examined. This particular insight underscores the pivotal role of gas selection in mitigating losses within the system, as evidenced by the comprehensive exergy study conducted within this research endeavor (Figure 11).

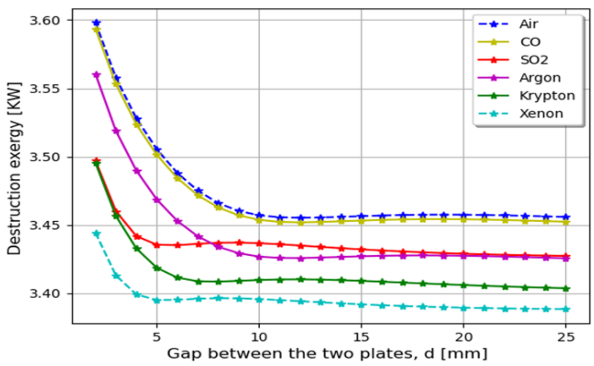

Figure 11. Exergy destruction in FPPV-T for different enclosed gases

The obtained exergy efficiency values for different gas-filled spaces are as follows: Xenon at 5 mm resulted in an efficiency of 0.5296 , followed closely by Krypton at the same spacing with a value of 0.5264. Argon at 10 mm displayed an efficiency of 0.5252, while SO_2 at 5 mm showed a value of 0.5240. The efficiency dropped slightly with CO at 10 mm, which yielded 0.5215, and air at 10 mm had an efficiency of 0.5210. These values signify the varying levels of exergy efficiency achieved across different gas types and spacings. Xenon and Krypton at smaller spacings notably showcased higher efficiency compared to Argon, SO_2, CO, and air at larger spacings (Figure 12).

Furthermore, the exergy analysis applied to the investigated PV-T system resulted in substantial improvements akin to those observed in the comprehensive combined efficiency analysis. Specifically, Xenon exhibited a significant exergy output of 3.8229 KW at a 5mm interspace, surpassing other gases. Krypton, Argon, and SO_2 yielded slightly lower exergy outputs of 3.7994 *KW* , 3.7912 KW , and 3.7845 KW , respectively, with interspaces of 5 mm, 10 mm, and 10 mm. Conversely, commonly used insulating gases such as air and CO within double-glazing showed comparatively lower exergy outputs of 3.7610 KW and 3.7643 KW, respectively, at the same 10mm spacing. These findings underscore the varying exergy outputs across different gases and spacings within the PV-T system, highlighting Xenon's superior exergy output compared to other gases evaluated (Figure 13).

The outcomes derived from this study were focused on identifying the most suitable spaces filled with specific insulating gases, employing two distinct methodologies. Firstly, a novel natural convection correlation was employed to assess the heat transfer coefficients and the overall heat loss coefficient. Secondly, both conventional and exerge methods were utilized to determine the optimal spaces between the Floating Plate Photovoltaic-Thermal (FPPV-T) plates. These combined approaches aimed to ascertain the ideal gas spacings that would optimize the system's thermal performance and minimize heat loss, utilizing advanced convection correlations and diverse analytical techniques.

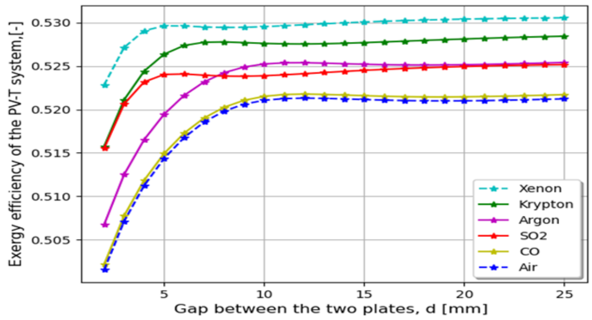

Figure 12. Exergy efficiency of the FPPV-T for different enclosed gases

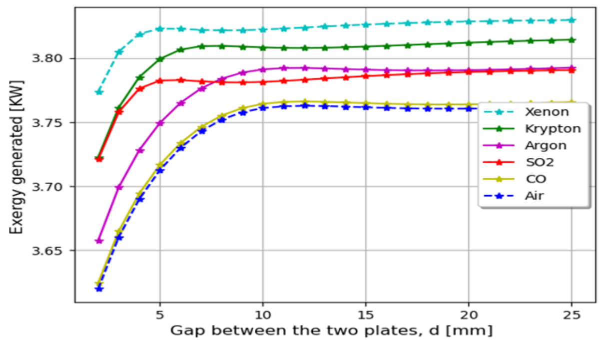

Figure 13. Exergy output by FPPV-T for different enclosed gases

5. CONCLUSIONS

The primary objective of this study was to enhance the efficiency of Flat Plate Photovoltaic-Thermal (FPPV-T) systems, opting for designs devoid of fins or artificial roughness, thus eliminating the need for high blowing power. The investigation focused on assessing the viability of noble gases as insulation alternatives compared to conventional air usage. In this context, noble gases such as Xenon, Krypton, Argon, sulfur dioxide (SO_2), and carbon monoxide (CO) were evaluated for their potential as insulating agents. These gases were specifically contained within the double paned glazing structure, positioned inside the solar collector's absorber and the inner glass. The study aimed to analyse the performance enhancements achievable by employing these noble gases as insulators within the FPPV-T system.

A mathematical framework was developed and executed using Spyder (Python 3.9) in the Anaconda environment. This model, constructed based on formulae for the energy balance with incorporating the correlation of Eismann [19], aimed to determine vital thermal parameters essential for evaluating the efficiency of a double-glazed Flat Plate Photovoltaic-Thermal (FPPV-T) system. Employing the more recent and refined Eismann correlation allowed for the calculation of coefficients for natural convection resulting from the gases trapped within the system. These coefficients, influenced by the temperatures of various PV-T components, played a critical role in the model. By integrating this advanced correlation and precision-based parameter estimation, the model facilitated a comprehensive assessment of the FPPV-T system's performance, emphasising improved accuracy and detailed thermal analyses.

The determination of the most efficient width for the gas-filled space within the double-glazing and above the absorber (PV model) to achieve the highest total combined efficiency involved the utilization of both conventional energy and exergy methodologies. Following this analysis, the optimized gap widths were established: 10mm for air and CO, 9mm for Argon and SO_2, 6mm for Krypton, and 5mm for Xenon. These specific gap dimensions were identified as the most favorable for achieving optimal total combined efficiency based on evaluations employing conventional energy and exergy approaches.

The gas-filled widths, particularly regarding Argon, were cross-referenced with the outcomes from Vestlund et al [76], showcasing identical optimal values. Moreover, the exergy study reaffirms the findings of the energy study, reinforcing the conclusion on the ideal gap width. Additionally, Antonanzas et al.'s research [34] presented consistent results under specific conditions. Additional tests using a smaller model are needed to validate these findings.

Theoretical analyses demonstrate significant enhancements in both useful heat energy and the total combined efficiency when substituting air with noble gases. Through appropriate gap configurations, it's evident that Xenon yields the highest efficiencies, closely trailed by Krypton, Argon, SO_2, CO. This highlights the considerable potential for performance improvement by employing these noble gases instead of air.

The exergy efficiency values obtained for various gas-filled spaces highlight Xenon's exceptional performance, registering an efficiency of 52.96%, closely followed by Krypton at 52.73%. Argon records an efficiency of 52.48%, while SO_2 demonstrates a value of 52.38%. However, there is a slight decrease in efficiency observed with CO at 52.15%, and air presents an efficiency of 52.10%. These exergy efficiency values emphasise the notable superiority of Xenon and Krypton compared to other gases, underlining their efficacy in optimizing energy utilization and minimizing losses within the system. Regarding the most suitable gas-filled spaces corresponding to these efficiencies, they align as follows: Xenon at 5 mm, Krypton at 6 mm, Argon, and SO_2 at 9 mm, and CO and air at 10 mm. These spacings correspond directly to the specific gases exhibiting the highest efficiencies, emphasizing their optimal utilization and performance within the system.

The use of Xenon as the filling gas in the FPPV-T system (with dimensions $\mathrm{L} = 15\ m$ and $\mathrm{W} = 2\ m$) results in a substantial rise in the useful heat energy collected. Specifically, it reaches 5.2924 kW, significantly surpassing the 3.977 kW achieved with air when utilizing the optimal gap widths. However, it's essential to emphasize that these results which would benefit from further experimental validation to ensure their accuracy and reliability.

REFERENCES

[1] Herrando, M., Markides, C.N., Hellgardt, K. (2014). A UK-based assessment of hybrid PV and solar-thermal systems for domestic heating and power: System performance. Applied Energy, 122: 288-309. https://doi.org/10.1016/J.APENERGY.2014.01.061

[2] Sathe, T.M., Dhoble A.S. (2017). A review on recent advancements in photovoltaic thermal techniques. Renewable and Sustainable Energy Reviews, 76: 645-672. https://doi.org/10.1016/j.rser.2017.03.075

[3] Nazri, N.S., Fudholi, A., Bakhtyar, B., Yen, C.H., Ibrahim, A., Ruslan, M.H., Mat, S., Sopian, K. (2018). Energy economic analysis of photovoltaic-thermal-thermoelectric (PVT-TE) air collectors. Renewable and Sustainable Energy Reviews, 92: 187-197. https://doi.org/10.1016/j.rser.2018.04.061

[4] Zohri, M., Ramadhan, W., Fudholi, A. (2022). Improvement potential and sustainability index of photovoltaic thermal solar air collector. International Journal of Heat and Technology, 40(3): 743-748. https://doi.org/10.18280/ijht.400312

[5] Hegazy, A.A. (2000). Comparative study of the performances of four photovoltaic/thermal solar air collectors. Energy Conversion and Management, 41(8): 861-881. https://doi.org/10.1016/S0196-8904(99)00136-3

[6] Maarof, H.A., Shamsi, M. (2022). Combining thermal and optical modeling to optimize the performance of a flat plate absorber at various locations in a solar air collector. Journal of Studies in Science and Engineering, 2(3): 31-51. https://doi.org/10.53898/JOSSE2022233

[7] Araújo, A. (2020). Thermo-hydraulic performance of solar air collectors with artificially roughened absorbers: A comparative review of semi-empirical models. Energies, 13(14): 3536. https://doi.org/10.3390/EN13143536

[8] Sukesh, N., Lakshmisagar, P.S., Kumar, G. (2015). Heat transfer analysis of fin performance for PVT absorber. Journal of Mechanical Engineering and Automation, 5(3B): 1-4. https://doi.org/10.5923/c.jmea.201502.01

[9] Ibrahim, A., Othman, M.Y., Ruslan, M.H., Mat, S., Sopian, K. (2011). Recent advances in flat plate photovoltaic/thermal (PV/T) solar collectors. Renewable and Sustainable Energy Reviews, 15(1): 352-365. https://doi.org/10.1016/j.rser.2010.09.024

[10] Rosli, M.A.M., Mat, S., Anuar, M.K., Sopian, K., Sulaiman, M.Y., Ellias, S. (2014). Progress on flat-plate water based of photovoltaic thermal (PV/T) system: A review. Iranica Journal of Energy & Environment, 5(4): 407-418. https://doi.org/10.5829/idosi.ijee.2014.05.04.09

[11] Michael, J.J., S, I., Goic, R. (2015). Flat plate solar photovoltaic-thermal (PV/T) systems: A reference guide. Renewable and Sustainable Energy Reviews, 51: 62-88. https://doi.org/10.1016/j.rser.2015.06.022

[12] Besheer, A.H., Smyth, M., Zacharopoulos, A., Mondol, J., Pugsley, A. (2016). Review on recent approaches for hybrid PV/T solar technology. International Journal of Energy Research, 40(15): 2038-2053. https://doi.org/10.1002/er.3567

[13] He, Y.T., Liu, R.M., Liu, J.H. (2013). Experimental research of photovoltaic/thermal (PV/T) solar systems. Applied Mechanics and Materials, 401-403: 146-150. https://doi.org/10.4028/www.scientific.net/AMM.401-403.146

[14] Chow, T.T. (2003). Performance analysis of

photovoltaic-thermal collector by explicit dynamic model. Solar Energy, 75(2): 143-152. https://doi.org/10.1016/j.solener.2003.07.001

[15] Zondag, H.A., de Vries, D.W., van Helden, W.G.J., van Zolingen, R.J.C., van Steenhoven, A.A. (2003). The yield of different combined PV-thermal collector designs. Solar Energy, 74(3): 253-269. https://doi.org/10.1016/S0038-092X(03)00121-X

[16] Pathak, M.J.M., Sanders, P.G., Pearce, J.M. (2014). Optimizing limited solar roof access by exergy analysis of solar thermal, photovoltaic, and hybrid photovoltaic thermal systems. Applied Energy, 120: 115-124. https://doi.org/10.1016/j.apenergy.2014.01.041

[17] Hollands, K.G.T., Unny, T.E., Raithby, G.D., Konicek, L. (1976). Free convective heat transfer across inclined air layers. Journal of Heat Transfer, 98(2): 189-193. https://doi.org/10.1115/1.3450517

[18] ElSherbiny, S.M., Raithby, G.D., Hollands, K.G.T. (1980). Heat transfer by natural convection across vertical and inclined air layers. ASME Journal of Heat and Mass Transfer, 104(1): 96-102. https://doi.org/10.1115/1.3245075

[19] Eismann, R. (2015). Accurate analytical modeling of flat plate solar collectors: Extended correlation for convective heat loss across the air gap between absorber and cover plate. Solar Energy, 122: 1214-1224. https://doi.org/10.1016/j.solener.2015.10.037

[20] Al-Damook, M., Khatir, Z., Al Qubeissi, M., Dixon-Hardy, D., Heggs, P.J. (2021). Energy efficient double-pass photovoltaic/thermal air systems using a computational fluid dynamics multi-objective optimisation framework. Applied Thermal Engineering, 194: 117010. https://doi.org/10.1016/j.applthermaleng.2021.117010

[21] Samant, T.S., Varshney, L. (2023). Flow rate for unbiased operation of photovoltaic thermal hybrid air heater in local climate. In 2022 IEEE International Power and Renewable Energy Conference (IPRECON), Kollam, India. https://doi.org/10.1109/IPRECON55716.2022.10059524

[22] Lamnatou, C., Chemisana, D. (2017). Photovoltaic/thermal (PVT) systems: A review with emphasis on environmental issues. Renewable Energy, 105: 270-287. https://doi.org/10.1016/j.renene.2016.12.009

[23] Abdul-Ganiyu, S., Quansah, D.A., Ramde, E.W., Seidu, R., Adaramola, M.S. (2020). Investigation of solar photovoltaic-thermal (PVT) and solar photovoltaic (PV) performance: A case study in Ghana. Energies, 13(11): 2701. https://doi.org/10.3390/en13112701

[24] Amori, K.E., Abd-AlRaheem, M.A. (2014). Field study of various air based photovoltaic/thermal hybrid solar collectors. Renewable Energy, 63: 402-414. https://doi.org/10.1016/j.renene.2013.09.047

[25] Miki, Y., Kohri, S., Takeyama, R., Aiso, K., Asai, S. (2006). Experimental studies on photovoltaic/thermal hybrid air-type solar collectors. Kitami Institute of Technology, 32(4): 67-73.

[26] Kim, J.H., Park, S.H., Kim, J.T. (2014). Experimental performance of a photovoltaic-thermal air collector. Energy Procedia, 48: 888-894. https://doi.org/10.1016/j.egypro.2014.02.102

[27] Fudholi, A., Musthafa, M.F., Ridwan, A., Yendra, R., Desvina, A.P., Rahmadeni, R., Suyono, T., Sopian, K. (2019). Energy and exergy analysis of air based photovoltaic thermal (PVT) collector: a review. International Journal of Electrical and Computer Engineering (IJECE), 9(1): 109. https://doi.org/10.11591/ijece.v9i1.pp109-117

[28] Mustapha, M., Fudholi, A., Yen, C.H., Ruslan, M.H., Sopian, K. (2018). Review on energy and exergy analysis of air and water based photovoltaic thermal (PVT) collector. International Journal of Power Electronics and Drive Systems, 9(3): 1367-1373. https://doi.org/10.11591/ijpeds.v9.i3.pp1367-1373

[29] Selimefendigil, F., Şirin, C. (2022). Energy and exergy analysis of a hybrid photovoltaic/thermal-air collector modified with nano-enhanced latent heat thermal energy storage unit. Journal of Energy Storage, 45: 103467. https://doi.org/10.1016/J.EST.2021.103467

[30] Joshi, A.S., Dincer, I., Reddy, B.V. (2011). Analysis of energy and exergy efficiencies for hybrid PV/T systems. International Journal of Low-Carbon Technologies, 6(1): 64-69. https://doi.org/10.1093/ijlct/ctq045

[31] Joshi, A.S., Tiwari, A. (2007). Energy and exergy efficiencies of a hybrid photovoltaic-thermal (PV/T) air collector. Renewable Energy, 32(13): 2223-2241. https://doi.org/10.1016/j.renene.2006.11.013

[32] Saloux, E., Teyssedou, A., Sorin, M. (2013). Analysis of photovoltaic (PV) and photovoltaic/thermal (PV/T) systems using the exergy method. Energy and Buildings, 67: 275-285. https://doi.org/10.1016/j.enbuild.2013.08.012

[33] Komilov, A. (2019). Simulation analysis of various applications of a combined photovoltaic panel with a single-channel natural flow heat collector. International Journal of Photoenergy, 2019: 8090817. https://doi.org/10.1155/2019/8090817

[34] Antonanzas, J., del Amo, A., Martinez-Gracia, A., Bayod-Rujula, A.A., Antonanzas-Torres, F. (2015). Towards the optimization of convective losses in photovoltaic-thermal panels. Solar Energy, 116: 323-336. https://doi.org/10.1016/j.solener.2015.04.013

[35] Srimanickam, B., Saranya, A. (2021). Thermal performance of single glazing flat plate photovoltaic thermal hybrid system with various air channels. Journal of Testing and Evaluation, 49(3): 2119-2150. https://doi.org/10.1520/JTE20170750

[36] Guruprasad, B., Srimanickam B., Natarajan U., Malayalamurthi R., Elango A. (2019). Performance investigation on various models on solar photovoltaic thermal (PVT) hybrid system. AIP Conference Proceedings, 2161(1): 020030. https://doi.org/10.1063/1.5127621

[37] Srimanickam, B., Vijayalakshmi, M.M., Natarajan, E. (2015). Experimental performance assessment of single glazing flat plate solar photovoltaic thermal (PV/T) hybrid system. Progress in Industrial Ecology, 9(2): 111-120. https://doi.org/10.1504/PIE.2015.073081

[38] Palaskar, V.N., Deshmukh, S. (2012). A critical review on enhancement in system performance of flat plate hybrid PV/T solar collector system. International Journal of Energy Science, 3(6). https://doi.org/10.14355/ijes.2013.0306.03

[39] Allan, J., Dehouche, Z., Stankovic, S., Mauricette, L. (2015). Performance testing of thermal and photovoltaic thermal solar collectors. Energy Science and Engineering,

3(4): 310-326. https://doi.org/10.1002/ese3.75
[40] Fudholi, A., Sopian, K., Yazdi, M.H., Ruslan, M.H., Ibrahim, A., Kazem, H.A. (2014). Performance analysis of photovoltaic thermal (PVT) water collectors. Energy Conversion and Management, 78: 641-651. https://doi.org/10.1016/J.ENCONMAN.2013.11.017
[41] Katiyar, M., van Balkom, M., Rindt, C.C.M., de Keizer, C., Zondag, H.A. (2017). Numerical model for the thermal yield estimation of unglazed photovoltaic-thermal collectors using indoor solar simulator testing. Solar Energy, 155: 903-919. https://doi.org/10.1016/J.SOLENER.2017.07.012
[42] Sultan, S.M., Tso, C.P., Efzan, E.M. (2018). A thermal performance study for different glazed water based photovoltaic thermal collectors. AIP Conference Proceedings, 2030(1): 020307. https://doi.org/10.1063/1.5066948
[43] Msirdi, N.K., Benabdellatif, M., Tina, G.M., Naamane, A., Dynamic, A.N. (2018). Dynamic coupled electrical and thermal model for PV-T solar energy collectors. In 2018 5th International Symposium on Environment-Friendly Energies and Applications (EFEA), Rome, Italy. https://doi.org/10.1109/EFEA.2018.8617098
[44] Omer, K.A., Zala, A.M. (2018). Experimental investigation of PV/thermal collector with theoretical analysis. Renewable Energy Focus, 27: 67-77. https://doi.org/10.1016/j.ref.2018.09.004
[45] Vettrivel, H., Mathiazhagan, P. (2017). Comparison study of solar flat plate collector with single and double glazing systems. International Journal of Renewable Energy Research, 7(1): 267-274. https://doi.org/10.20508/IJRER.V7I1.5397.G6985
[46] Ehyaei, M.A., Farshin, B. (2017). Optimization of photovoltaic thermal (PV/T) hybrid collectors by genetic algorithm in Iran’s residential areas. Advances in Energy Research, 5(1): 31-55. https://doi.org/10.12989/eri.2017.5.1.031
[47] Lari, K., Tarokh, A., Naghizadeh, M. (2019). Gas radiative effects on gas-filled flat plate solar collectors. Canadian Journal of Physics, 97(10): 1115-1124. https://doi.org/10.1139/cjp-2018-0878
[48] Tchinda, R. (2009). A review of the mathematical models for predicting solar air heaters systems. Renewable and Sustainable Energy Reviews, 13(8): 1734-1759. https://doi.org/10.1016/j.rser.2009.01.008
[49] Dubey, S., Sarvaiya, J.N., Seshadri, B. (2013). Temperature dependent photovoltaic (PV) efficiency and its effect on PV production in the world - A review. Energy Procedia, 33: 311-321. https://doi.org/10.1016/j.egypro.2013.05.072
[50] Amori, K.E., Taqi Al-Najjar, H.M. (2012). Analysis of thermal and electrical performance of a hybrid (PV/T) air based solar collector for Iraq. Applied Energy, 98: 384-395. https://doi.org/10.1016/j.apenergy.2012.03.061
[51] Aste, N., del Pero, C., Leonforte, F. (2014). Water flat plate PV-thermal collectors: A review. Solar Energy, 102: 98-115. https://doi.org/10.1016/j.solener.2014.01.025
[52] Shahsavar, A., Ameri, M. (2010). Experimental investigation and modeling of a direct-coupled PV/T air collector. Solar Energy, 84(11): 1938-1958. https://doi.org/10.1016/J.SOLENER.2010.07.010
[53] Evans, D.L. (1981). Simplified method for predicting photovoltaic array output. Solar Energy, 27(6): 555-560. https://doi.org/10.1016/0038-092X(81)90051-7
[54] Notton, G., Cristofari, C., Mattei, M., Poggi, P. (2005). Modelling of a double-glass photovoltaic module using finite differences. Applied Thermal Engineering, 25(17-18): 2854-2877. https://doi.org/10.1016/j.applthermaleng.2005.02.008
[55] Tiwari, G.N., Tiwari, A., Shyam. (2016). Handbook of Solar Energy. https://doi.org/10.1007/978-981-10-0807-8
[56] Choudhury, C., Chauhan, P.M., Garg, H.P. (1995). Design curves for conventional solar air heaters. Renewable Energy, 6(7): 739-749. https://doi.org/10.1016/0960-1481(95)00007-7
[57] Duffie, J., Beckman, W. (2013). Solar Engineering of Thermal Processes. Fourth Ed., John Wiley & Sons, New Jersey.
[58] Al-Waeli, A.H.A., Kazem, H.A., Chaichan, M.T., Sopian, K. (2019). Photovoltaic/Thermal (PV/T) Systems: Principles, Design, and Applications. https://doi.org/10.1007/978-3-030-27824-3
[59] Tonui, J.K., Tripanagnostopoulos, Y. (2007). Air-cooled PV/T solar collectors with low cost performance improvements. Solar Energy, 81(4): 498-511. https://doi.org/10.1016/J.SOLENER.2006.08.002
[60] Aste, N., Chiesa, G., Verri, F. (2008). Design, development and performance monitoring of a photovoltaic-thermal (PVT) air collector. Renewable Energy, 33(5): 914-927. https://doi.org/10.1016/J.RENENE.2007.06.022
[61] Berdahi, P., Martin, M. (1982). Emissivity of Clear Skies. LBL Publications.
[62] ASHRAE Handbook of Fundamentals. (2017). Chapter 1 psychometrics, 1.10, Chapter 15 Fenestration, 15.3, Atlanta, GA, USA.
[63] Buck, A.L. (1981). New equations for computing vapor pressure and enhancement factor. Journal of Applied Meteorology and Climatology, 20(12): 1527-1532.
[64] Lide, D.R. (2005). Pressure and temperature dependence of liquid density. In CRC Handbook of Chemistry and Physics, Internet Version 2005, David R. Lide, ed., CRC Press, Boca Raton, FL.
[65] Air-Liquide. (2023). Physical Data of Gases. https://th.airliquide.com/sites/al_th/files/2023-07/gas-specification-v12.pdf.
[66] Shah, R.K., London, A.L. (1978). Rectangular ducts. Laminar Flow Forced Convection in Ducts, 196-222. https://doi.org/10.1016/b978-0-12-020051-1.50012-7
[67] Gnielinski, V. (1976). New equations for heat and mass transfer in turbulent pipe and channel flow. Forschung im Ingenieurwesen, 41(1): 8-16.
[68] Frank, K., Raj, M.M., Mark, S.B. (2002). Principles of heat transfer. Applied Mechanics Reviews, 55(5): B100-B102. https://doi.org/10.1115/1.1497490
[69] Sarhaddi, F., Farahat, S., Ajam, H., Behzadmehr, A., Mahdavi Adeli, M. (2010). An improved thermal and electrical model for a solar photovoltaic thermal (PV/T) air collector. Applied Energy, 87(7): 2328-2339. https://doi.org/10.1016/j.apenergy.2010.01.001
[70] Ibrahim, A., Fudholi, A., Sopian, K., Othman, M.Y., Ruslan, M.H. (2014). Efficiencies and improvement potential of building integrated photovoltaic thermal (BIPVT) system. Energy Conversion and Management, 77: 527-534. https://doi.org/10.1016/J.ENCONMAN.2013.10.033
[71] Agrawal, S., Tiwari, G.N. (2011). Energy and exergy

analysis of hybrid micro-channel photovoltaic thermal module. Solar Energy, 85(2): 356-370. https://doi.org/10.1016/J.SOLENER.2010.11.013
[72] Sardarabadi, M., Hosseinzadeh, M., Kazemian, A., Passandideh-Fard, M.(2017). Experimental investigation of the effects of using metal-oxides/water nanofluids on a photovoltaic thermal system (PVT) from energy and exergy viewpoints. Energy, 138: 682-695. https://doi.org/10.1016/J.ENERGY.2017.07.046
[73] Arslan, E., Aktaş, M. (2020). 4E analysis of infrared-convective dryer powered solar photovoltaic thermal collector. Solar Energy, 208: 46-57. https://doi.org/10.1016/j.solener.2020.07.071
[74] Fudholi, A., Zohri, M., Jin, G.L., Ibrahim, A., Yen, C.H., Othman, M.Y., Ruslan, M.H., Sopian, K. (2018). Energy and exergy analyses of photovoltaic thermal collector with ∇-groove. Solar Energy, 159: 742-750. https://doi.org/10.1016/j.solener.2017.11.056
[75] Nazri, N.S., Fudholi, A., Mustafa, W., Yen, C.H., Mohammad, M., Ruslan, M.H., Sopian, K. (2019). Exergy and improvement potential of hybrid photovoltaic thermal/thermoelectric (PVT/TE) air collector. Renewable and Sustainable Energy Reviews, 111: 132-144. https://doi.org/10.1016/J.RSER.2019.03.024
[76] Vestlund, J., Dalenbäck, J.O., Rönnelid, M. (2012). Thermal and mechanical performance of sealed, gas-filled, flat plate solar collectors. Solar Energy, 86(1): 13-25. https://doi.org/10.1016/j.solener.2011.08.023

NOMENCLATURE

A_c	collector area, m^2
A_{pv}	area of PV cell m^2
A_p	area of absorber plate m^2
A_e	side edges surface m^2
L	air duct length, m
W	air duct width, m
C_f	Fluid(air) specific heat $J/(kg.k)$
C_p	specific heat at constant pressure $J/(kg.k)$
D_h	hydraulic diameter, m
d	inner glass to outer glass distance/inner glass to absorber plate distance, m
e	thickness, m
F	Packing factor
F'	collector efficiency factor
g	gravitational acceleration $m/(s^2)$
F_r	collector heat removal factor
H	air duct height, m
h_r	heat radiation coefficient, $W/(m^2.k)$
h_c	forced convection coefficient, $W/(m^2.k)$
h_{nc}	natural convection coefficient, $W/(m^2.k)$
h_{inl}	solar collector inlet enthalpy $W/(m^2.k)$
h_{out}	solar collector outlet enthalpy, $W/(m^2.k)$
h_w	heat transfer coefficient due to wind, $W/(m^2.k)$
K_{eq}	glass equivalent heat transfer coefficient, $W/(m^2.k)$
U	heat loss coefficient, $W/(m^2.k)$
U_b	collector back heat loss coefficient, $W/(m^2.k)$
U_L	collector overall heat loss coefficient, $W/(m^2.k)$
U_T	collector top heat loss coefficient, $W/(m^2.k)$
K	thermal conductivity, $W/(m.k)$
$\dot{m}_f$	air mass flow rate, kg/s
Nu	Nusselt number
Pr	Prandtl number
R_a	Reynolds number
$R_a{}'$	Rayleigh number for inclined planes
p_{fan}	fan pressure, Pa
p_w	partial vapor pressure of air, Pa
p_{sw}	saturation vapor pressure of air, Pa
Δp	pressure drop across the collector length, Pa
$\emptyset_u$	useful hout energy of the solar collector, W
t	day hour, h
r	air duct surface roughness, m
S	energy absorbed by per unit area, W/m^2
S_1	energy absorbed by the inner glass, W/m^2
S_2	energy absorbed by the outer glass, W/m^2
S_p	energy absorbed by the absorber plate, W/m^2
S_{inl}	solar collector inlet entropy, J/K
S_{out}	solar collector outlet entropy, J/K
u	air velocity, m/s
V_w	wind velocity, m/s
T_{g1}	inner glazing temperature, K
T_{g2}	outer glazing temperature, K
T_a	ambient temperature, K
T_{dp}	dew point temperature, K
T_s	sky temperature, K
T_m	mean temperature, K
T_{sun}	sun temperature, K
$\acute{E}$	exergy rate, W

Greek symbols

σ	Stefan-Boltzmann constant
α	absorptance
$\alpha_{D\ gas}$	thermal diffusivity for gases, m^2/s
α^*	aspect ratio (duct height to width ratio)
β	collector tilt angle, deg
β'	gas thermal expansion coefficient, K^{-1}
τ	transmittance
ε	emissivity
μ	dynamic viscosity, Pa.s
η_c	The total combined efficiency
η_{th}	the thermal efficiency
η_{Pv}	The electrical efficiency of the PV module
η_{EPv}	The equivalent electrical efficiency of PV
η_{fan}	fan efficiency
η_m	mechanical efficiency
η	Exergy efficiency
$\mathcal{F}$	friction factor
υ	kinematic viscosity, m^2/s
Φ	relative humidity (RH)

Subscripts

a	ambient
f	flowing air, fluid
ei	edge insulation
des	destroyed
ins	insulation
Bp	bottom plate
p	absorber plate

inl, i	inlet
out, o	outlet
u, p	for useful exergy with pressure drop
$f - p$	air flow to absorber plate
$Bp - f$	bottom plate to air flow
$g_1 - a$	inner glass to ambience
$g_2 - a$	outer glass to ambience
$g_2 - g_1$	inner glass to outer glass
$Bp - g_1$	absorber plate to inner glass
$p - Bp$	absorber plate to bottom plate